ChemComm

A π-extended tercarbazole-core multi-resonance delayed fluorescence emitter exhibiting efficient narrowband yellow electroluminescence

Journal:	*ChemComm*
Manuscript ID	CC-COM-07-2023-003241.R1
Article Type:	Communication

COMMUNICATION

A π-extended tercarbazole-core multi-resonance delayed fluorescence emitter exhibiting efficient narrowband yellow electroluminescence

Received 00th January 20xx,
Accepted 00th January 20xx

DOI: 10.1039/x0xx00000x

Rajendra Kumar Konidena,*[a,b] Minlang Yang[a] and Takuma Yasuda*[a]

Herein, a simple and versatile molecular design for long-wavelength (>550 nm) multi-resonance thermally activated delayed fluoresence emitters is reported. Extending a fully fused polycyclic π-system with an additional *para*-N-π-N conjugation induces narrowband bright-yellow photoluminescence and electroluminescence emissions at ~560 nm.

Thermally activated delayed fluorescence (TADF) materials, which allow 100% exciton utilization for electroluminescence (EL), have been extensively studied as promising noble-metal-free emitters in organic light-emitting diodes (OLEDs).[1] Among them, boron- and nitrogen-embedded polycyclic aromatic hydrocarbons (B,N-PAHs) have recently attracted significant attention because of their excellent narrowband emission features,[2–15] making B,N-PAHs suitable for application in ultra-high-definition displays. The complementary multi-resonance (MR) effect of adjacent B and N atoms endows B,N-PAHs with atomically separated highest occupied molecular orbital (HOMO) and lowest unoccupied molecular orbital (LUMO) distributions, leading to a small singlet–triplet (S_1–T_1) energy gap (ΔE_{ST}) for reverse intersystem crossing (RISC) and enabling TADF emission.[2] Moreover, rigid B,N-PAH molecular frameworks enable extremely narrowband emissions with full width at half maxima (FWHM) of ≤ 50 nm and high photoluminescence quantum yields (Φ_{PL}) owing to suppressed structural relaxation and vibronic coupling in the excited states.

To date, a variety of MR-TADF emitters with excellent EL color purity and external quantum efficiency (EQE) in OLEDs have been reported.[4] However, with a few exceptions,[5–13] most of MR-TADF systems based on B,N-PAH frameworks emit in the blue-to-green region; to facilitate a wide range of applications, a color gamut expansion (especially at >550 nm) is required. To this end, various peripheral molecular modifications have been applied on the simplest B,N-PAH skeleton, **BBCz-SB** (Fig. 1).[5] Introducing auxiliary electron-donor or -acceptor units onto the HOMO- or LUMO-dominated carbons in the **BBCz-SB** periphery varies the corresponding energy levels, causing a bathochromic shift of the emission band.[3,5–8] Alternatively, highly π-extended B,N-PAHs with strong *para*-N-π-N and *para*-B-π-B conjugations have been developed as narrowband red/deep-red emitters.[5,9–11] However, these designs involve complicated syntheses and increased molecular weights, which are detrimental to OLED applications.

Herein, a simple and versatile molecular design for achieving long-wavelength (>550 nm) narrowband emission is reported. In the newly designed π-extended MR-TADF emitter, **CzCzB** (Fig. 1), an additional *para*-N-π-N conjugation between the central fused carbazole subunit and an outer carbazole subunit facilitates charge delocalization over the entire B,N-PAH framework; this lowers the S_1 and T_1 energies, causing a significant emission-band bathochromic shift. As expected, **CzCzB** exhibited narrowband yellow emission with a peak at 558 nm in toluene, which was red-shifted by ~70 and 60 nm in relation to that of the parent compound **BBCz-SB**[5] and its isomeric compound **NBNP**[14] (with *para*-B-π-N conjugation), respectively. Furthermore, **CzCzB**-based OLEDs showed narrowband bright-yellow EL with a high maximum EQE (EQE_{max}) of 19.0%.

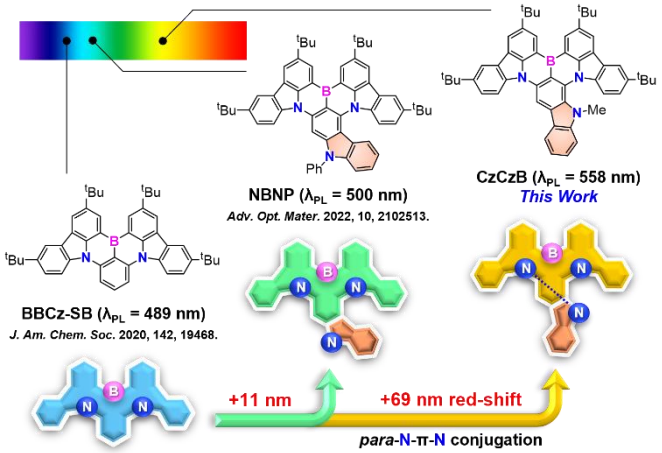

Fig 1. Design of a yellow MR-TADF emitter, **CzCzB**, via ring-fusion π-extension involving *para*-N-π-N conjugation.

[a] *Institute for Advanced Study, Kyushu University, Fukuoka, Japan. E-mail: yasuda@ifrc.kyushu-u.ac.jp*
[b] *Department of Chemistry, Faculty of Engineering and Technology, SRM Institute of Science and Technology, Kattankulathur, Chennai, 603203, Tamil Nadu, India. Email: rajendrk1@srmist.edu.in*

†Electronic Supplementary Information (ESI) available: DOI: 10.1039/x0xx00000x

As outlined in Scheme 1, **CzCzB** was synthesized via a three-step reaction, using pinacolborate **1**[15] as the starting material (details are available in the ESI†). The Pd-catalyzed Suzuki–Miyaura coupling of **1** with 1-bromo-2-nitrobenzene, followed by Cadogan cyclization using PPh_3,[16] afforded **3** with a 9,1′:3′,9″-tercarbazole core. Subsequently, the NaH-mediated nucleophilic substitution of **3** with iodomethane produced **CzCzB** in good yields. As indicated by thermogravimetric analysis, **CzCzB** with a robust 11-ring-fused skeleton exhibited excellent thermal stability with a 5% weight-loss temperature (T_d) of 428 °C (ESI†). The proposed synthetic strategy is concise and versatile; hence, it can be used to develop analogs with a wide emission color gamut.

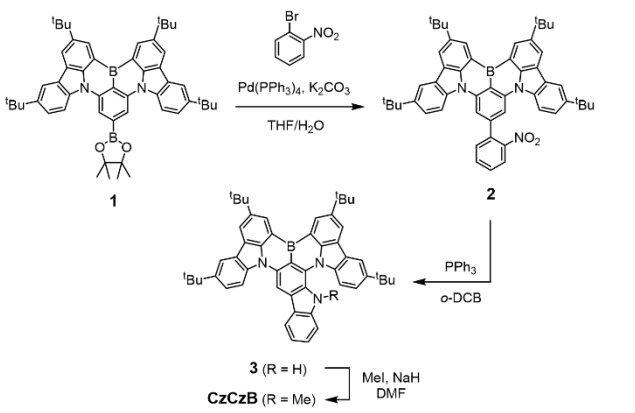

Scheme 1 Synthetic route for the 11-ring-fused **CzCz-B**.

Fig. 2 shows the photophysical spectroscopic properties of **CzCzB** in dilute toluene solution and doped thin films embedded in a 3,3′-di(carbazole-9-yl)biphenyl (mCBP) host; the corresponding data are listed in Table 1. The solution absorption spectrum showed an intense band centered at 518 nm with a molar absorption coefficient of ~3×10^4 M^{-1} cm^{-1} (Fig. 2a), which corresponds to the HOMO→LUMO electronic transition involving mixed short- and long-range charge transfer (CT) (ESI†). The solution and doped films of **CzCzB** exhibited similar bright-yellow photoluminescence (PL), with emission peaks (λ_{PL}) at 558 and 559 nm, and Φ_{PL} values of 89% and 87%, respectively (Fig. 2b,c). Notably, for **CzCzB**, ring-fusion π-extension caused a large red shift of λ_{PL} by ~70 and ~60 nm with respect to the parent compound **BBCz-SB** (λ_{PL} = 489–490 nm) and analogous compound **NBNP** (λ_{PL} = 500 nm). The significant bathochromic shift of **CzCzB** compared to **NBNP** can be attributed the conjugation connectivity of the N atom on the central carbazole moieties. In the case of **NBNP**, the N atom is located in the *para*-position to the B atom, whereas in **CzCzB** it is shifted to the *para*-position relative to one of the carbazole N atoms of the parent B,N-PAH core. As a result, the CT character of **CzCzB** was enhanced through *para*-N-π-N conjugation, resulting in larger bathochromic shift compared to **NBNP**. However, for **CzCzB**, because of long-range CT contributions, the spectral FWHM of the PL spectra increased to 47–48 nm, which was larger than that of **NBNP** (29 nm). The S_1 and T_1 excitation energies (E_S and E_T) of **CzCzB** were estimated to be 2.22 and 2.02 eV, respectively, from the fluorescence and phosphorescence peaks (ESI†), affording a ΔE_{ST} of 0.20 eV. Although this ΔE_{ST} value is slightly larger than those of state-of-the-art MR-TADF emitters, it is sufficiently small to induce effective RISC ($T_1 \rightarrow S_1$) and TADF. Indeed, the **CzCzB** solution and doped films both showed distinct double-exponential transient PL decays comprising prompt and delayed fluorescence (Fig. 2d and ESI†). The prompt and delayed fluorescence lifetimes (τ_p and τ_d) of **CzCzB** were estimated to be 8.9 ns and 217 μs, respectively, with fractional quantum yields (Φ_p and Φ_d) of 55% and 32%, respectively, for the doped film. Based on experimental data, the radiative decay rate constant (k_r) of **CzCzB** was calculated to be ~6×10^7 s^{-1}, whereas the intersystem crossing (ISC) and RISC rate constants (k_{ISC} and k_{RISC}) were estimated to be ~5×10^7 and ~6×10^3 s^{-1}, respectively. The RISC process in **CzCzB** was slower than that in **BBCz-SB** and **NBNP**, presumably owing to its slightly larger ΔE_{ST} (0.20 eV (**CzCzB**) > 0.15 eV (**BBCz-SB**) > 0.09 eV (**NBNP**)).

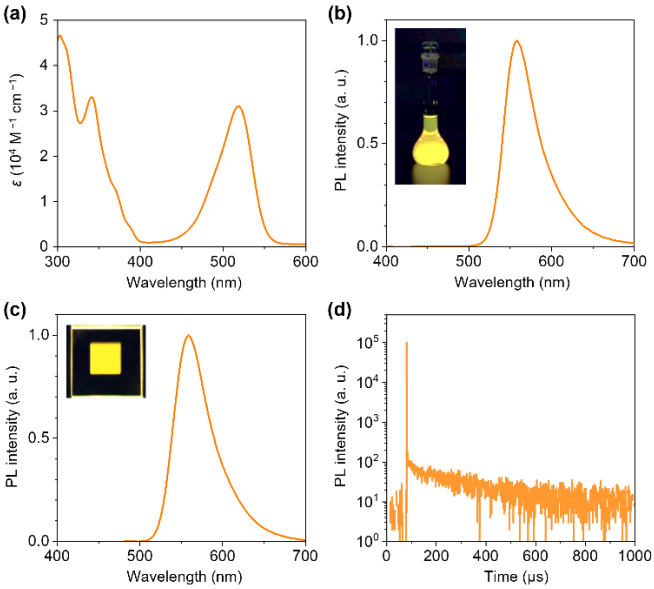

Fig. 2 (a) UV–vis absorption and (b) PL spectra of **CzCzB** in deoxygenated toluene (10^{-5} M) (inset: a photograph of the bright-yellow emission under UV illumination at 365 nm). (c) Steady-state PL spectrum (inset: an emission image) and (d) transient PL decay profile of a 1 wt%-CzCzB:mCBP doped film, acquired at 300 K.

Table 1 Photophysical Data of **CzCzB**

	solution[a]	doped film[b]
λ_{PL}[c] (nm)	558	559
FWHM[d] (nm/eV)	47/0.18	48/0.19
Φ_{PL}[e] (%)	89	87
Φ_p/Φ_d[f] (%)	51/37	55/32
τ_p/τ_d[g] (ns/μs)	8.8/307	8.9/217
k_r[h] (s^{-1})	5.9×10^7	6.2×10^7
k_{ISC}[i] (s^{-1})	5.5×10^7	5.0×10^7
k_{RISC}[j] (s^{-1})	5.0×10^3	5.9×10^3

[a]Measured in a deoxygenated toluene solution (10^{-5} M) at 300 K. [b]Measured using a 1 wt%-doped thin film with an mCBP host at 300 K under N_2. [c]PL emission maximum. [d]Full width at half maximum of the PL spectrum (in wavelength and energy). [e]Absolute PL quantum yield evaluated using an integrating sphere. [f]Fractional quantum yields for prompt fluorescence (Φ_p) and delayed fluorescence (Φ_d): $\Phi_p + \Phi_d = \Phi_{PL}$. [g]Emission lifetimes for prompt fluorescence (τ_p) and delayed fluorescence (τ_d). [h]Radiative decay rate constant for $S_1 \rightarrow S_0$: $k_r = \Phi_p/\tau_p$. [i]ISC rate constant for $S_1 \rightarrow T_1$: $k_{ISC} = (1 - \Phi_p)/\tau_p$. [j]RISC rate constant for $T_1 \rightarrow S_1$: $k_{RISC} = \Phi_d/(k_{ISC} \cdot \tau_p \cdot \tau_d \cdot \Phi_p)$.

Natural transition orbital (NTO) analysis was conducted to elucidate the excited-state characteristics of **CzCzB** (Fig. 3). For the S_1 state, the hole and electron wave functions resided in different segments as a whole, indicating long-range CT. Simultaneously, the original MR-induced short-range CT, characterized by atomically separated orbital distributions, was retained to a significant degree. These mixed CT characteristics enabled **CzCzB** to exhibit a significant PL bathochromic shift, while maintaining its intrinsic narrowband spectral features. The S_1 and T_1 states showed similar distributions of hole and electron wave functions; negligible orbital angular momentum variation resulted in an extremely small T_1–S_1 spin–orbit coupling (SOC) value ($\langle S_1|\hat{H}_{SOC}|T_1\rangle$ = 0.02 cm^{-1}). The higher-order T_2 state was energetically close to the S_1 state and showed a locally excited character dominated by one carbazole fragment; this can represent another spin-flip RISC channel with enhanced SOC ($\langle S_1|\hat{H}_{SOC}|T_2\rangle$ = 0.18 cm^{-1}).

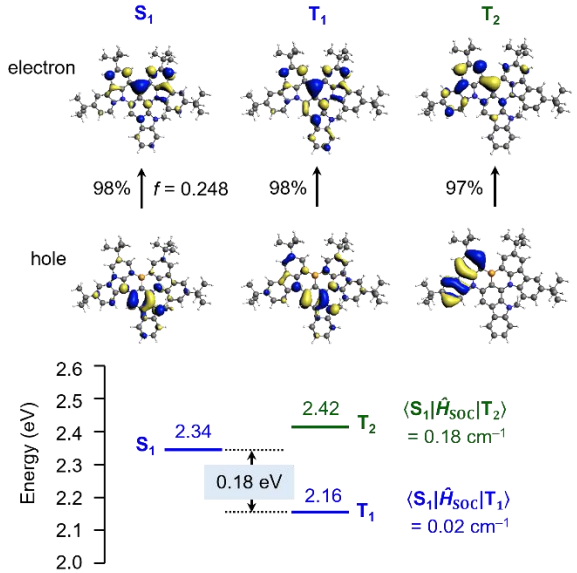

Fig. 3 NTOs for the excited singlet (S_1) and triplet (T_n) states of **CzCzB**, along with the simulated energy-level diagram for **CzCzB**. The NTOs, S_1 and T_n excitation energies, and associated T_n–S_1 spin–orbit coupling matrix elements are calculated at the B3LYP/DZP level.

The production of yellow MR-TADF emitter, **CzCzB**, prompted the fabrication of OLEDs, toward the investigation of its EL performance. OLEDs with the following layer sequence were fabricated: indium tin oxide (ITO)/HAT-CN (10 nm)/TAPC (40 nm)/mCBP (10 nm)/1 wt%-**CzCzB**:mCBP (20 nm)/B3PyPB (50 nm)/Liq (1 nm)/Al (100 nm) (the material structures and energy-level diagram of the device are provided in the ESI†). As depicted in Fig. 4a, the **CzCzB**-based OLED exhibited narrowband EL, with a peak (λ_{EL}) at 559 nm and an FWHM of 48 nm (0.19 eV), consistent with the corresponding PL spectrum (Fig. 2c). Narrowband EL resulted in excellent yellow color purity, as indicated by the Commission Internationale de l'Éclairage (CIE) chromaticity coordinates of (0.43, 0.56) (Fig. 4b). Moreover, the **CzCzB**-based device showed a high EQE_{max} of 19.0% (Fig. 4c,d), indicating the utilization of both electrogenerated S_1 and T_1 excitons for EL emission. However, large efficiency roll-offs were observed at practical brightness, and the EQE values decreased to 9.7% and 6.7% at 100 and 1000 cd m^{-2}, respectively. This behavior can be attributed to the long triplet exciton lifetime, which extends over several hundred microseconds owing to the slow RISC of **CzCzB**. An application of TADF-sensitized fluorescence mechanisms can improve the efficiency roll-off and device performance;[17,18] relevant device engineering studies are currently underway.

In summary, we proposed a simple and versatile molecular design for long-wavelength MR-TADF emitters, which was used to develop a narrowband yellow-emissive material, **CzCzB**. **CzCzB**-based OLEDs displayed narrowband bright-yellow EL with a high EQE_{max} of 19.0% and spectral FWHM of 48 nm. These results will open new frontiers in the development of high-efficiency long-wavelength MR-TADF emitters.

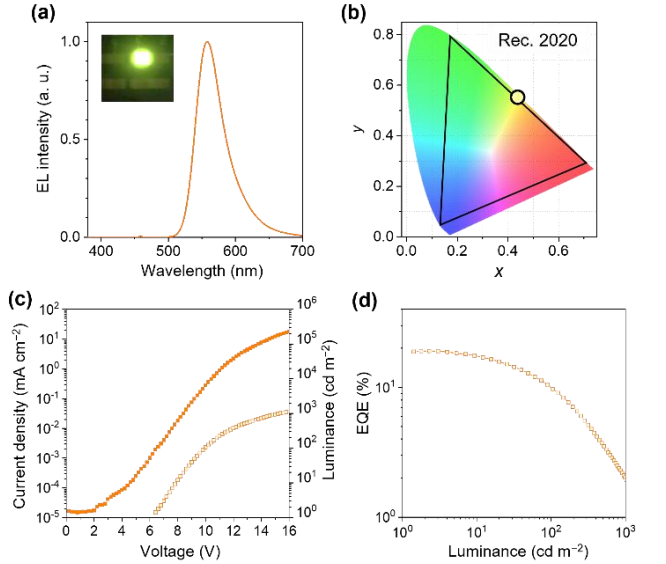

Fig. 4 EL characteristics of **CzCzB**-based OLEDs: (a) EL spectrum (inset: yellow EL image) acquired at 100 cd m^{-2}, (b) EL color coordinates in the CIE chromaticity diagram, (c) current density–voltage–luminance (*J*–*V*–*L*) characteristics, and (d) EQE–*L* plots.

This work was supported in part by Grant-in-Aid for JSPS KAKENHI (Grant No. JP21H04694 and JP22F21030) and JST CREST (Grant No. JPMJCR21O5). R.K.K. acknowledges the JSPS Postdoctoral Fellowships for Research in Japan. The authors are grateful for the support provided by the Cooperative Research Program of "Network Joint Center for Materials and Devices" and the computer facilities at the Research Institute for Information Technology, Kyushu University.

Author Contributions

R.K.K., M.Y., and T.Y. conceptualized the project. R.K.K. synthesized materials and performed quantum chemical calculations. M.Y. performed photophysical analysis and device evaluations. R.K.K., M.Y., and T.Y. co-wrote the manuscript. T.Y. supervised the entire research project.

Conflicts of interest

There are no conflicts to declare.

References

1. For the earliest TADF-OLEDs, see: a) A. Endo, K. Sato, K. Yoshimura, T. Kai, A. Kawada, H. Miyazaki and C. Adachi, *Appl. Phys. Lett.*, 2011, **98**, 083302; b) S. Y. Lee, T. Yasuda, H. Nomura and C. Adachi, *Appl. Phys. Lett.*, 2012, **101**, 093306; c) H. Uoyama, K. Goushi, K. Shizu, H. Nomura and C. Adachi, *Nature*, 2012, **492**, 234.
2. a) T. Hatakeyama, K. Shiren, K. Nakajima, S. Nomura, S. Nakatsuka, K. Kinoshita, J. Ni, Y. Ono and T. Ikuta, *Adv. Mater.,* 2016, **28**, 2777; b) Y. Kondo, K. Yoshiura, S. Kitera, H. Nishi, S. Oda, H. Gotoh, Y. Sasada, M. Yanai and T. Hatakeyama, *Nat. Photonics*, 2019, **13**, 678; c) K. Matsui, S. Oda, K. Yoshiura, K. Nakajima, N. Yasuda and T. Hatakeyama, *J. Am. Chem. Soc.*, 2018, **140**, 1195.
3. a) X. Liang, Z.-P. Yan, H.-B. Han, Z.-G. Wu, Y.-X. Zheng, H. Meng, J.-L. Zuo and W. Huang, *Angew. Chem. Int. Ed.*, 2018, **57**, 11316; b) S. H. Han, J. H. Jeong, J. W. Yoo and J. Y. Lee, *J. Mater. Chem. C*, 2019, **7**, 3082; c) Y. Zhang, D. Zhang, J. Wei, Z. Liu, Y. Lu and L. Duan, *Angew. Chem. Int. Ed.*, 2019, **58**, 16912; d) S. M. Suresh, E. Duda, D. Hall, Z. Yao, S. Bagnich, A. M. Z. Slawin, H. Bäassler, D. Beljonne, M. Buck, Y. Olivier, A. Köhler and E. Zysman-Colman, *J. Am. Chem. Soc.*, 2020, **142**, 6588; e) Y. Xu, Z. Cheng, Z. Li, B. Liang, J. Wang, J. Wei, Z. Zhang and Y. Wang, *Adv. Opt. Mater.*, 2020, **8**, 1902142.
4. For recent reviews, see: a) H. J. Kim and T. Yasuda, *Adv. Opt. Mater*. 2022, **10**, 2201714.; b) R. K. Konidena and K. R. Naveen, *Adv. Photon. Res*. 2022, **3**, 2200201; c) K. R. Naveen, P. Palanisamy, M. Y. Chae and J. H. Kwon, *Chem. Commun.*, 2023, **59**, 3685; d) S. M. Suresh, D. Hall, D. Beljonne, Y. Olivier and E. Zysman-Colman, *Adv. Funct. Mater.,* 2020, **30**, 1908677.
5. M. Yang, I. S. Park and T. Yasuda, *J. Am. Chem. Soc.*, 2020, **12**, 19468.
6. M. Yang, S. Shikita, H. Min, I. S. Park, H. Shibata, N. Amanokura and T. Yasuda, *Angew. Chem. Int. Ed.*, 2021, **60**, 23142.
7. Y. Liu, X. Xiao, Y. Ran, Z. Bin and J. You, *Chem. Sci*., 2021, **12**, 9408.
8. Y. Qi, W. Ning, Y. Zou, X. Cao, S. Gong and C. Yang, *Adv. Funct. Mater.*, 2021, **31**, 2102017.
9. Y. Zhang, D. Zhang, T. Huang, A. J. Gillett, Y. Liu, D. Hu, L. Cui, Z. Bin, G. Li, J. Wei and L. Duan, *Angew. Chem. Int. Ed.*, 2021, **60**, 20498.
10. Y. Zou, J. Hu, M. Yu, J. Miao, Z. Xie, Y. Qiu, X. Cao and C. Yang, *Adv. Mater.*, 2022, **34**, 2201442.
11. Y. Wang, K. Zhang, F. Chen, X. Wang, Q. Yang, S. Wang, S. Shao and L. Wang, *Chin. J. Chem*. 2022, **40**, 2671.
12. Y.-C. Cheng, X.-C. Fan, F. Huang, X. Xiong, J. Yu, K. Wang, C.-S. Lee and X. H. Zhang, *Angew. Chem. Int. Ed*., 2022, **61**, e202212575.
13. W. Yang, J. Miao, F. Hu, Y. Zou, C. Zhong, S. Gong and C. Yang, *Adv. Funct. Mater*., 2023, **33**, 2213056.
14. X.-F. Luo, H.-X. Ni, H.-L. Ma, Z.-Z. Qu, J. Wang, Y.-X. Zheng and J.-L. Zuo, *Adv. Opt. Mater.*, 2022, **10**, 2102513.
15. a) M. Yang, R. K. Konidena, S. Shikita and T. Yasuda, *J. Mater. Chem. C*, 2023, **11**, 917; b) Y. Xu, C. Li, Z. Li, J. Wang, J. Xue, Q. Wang, X. Cai and Y. Wang, *CCS Chem*, 2022, **4**, 2065.
16. For reviews, see: a) J. I. G. Cadogan and R. K. Mackie, *Chem. Soc. Rev.*, 1974, **3**, 87; b) A. W. Freeman, M. Urvoy and M. E. Criswell, *J. Org. Chem.*, 2005, **70**, 5014; c) M. Kaur and R. Kumar, *Asian J. Org. Chem.*, 2022, **11**, e202200092.
17. C.-Y. Chan, M. Tanaka, Y.-T. Lee, Y.-W. Wong, H. Nakanotani, T. Hatakeyama and C. Adachi, *Nat. Photonics*, 2021, **15**, 203.
18. S. O. Jeon, K. H. Lee, J. S. Kim, S.-G. Ihn, Y. S. Chung, J. W. Kim, H. Lee, S. Kim, H. Choi and J. Y. Lee, *Nat. Photonics*, 2021, **15**, 208.